Journal of Chromatography B, 879 (2011) 3337–3343

Contents lists available at ScienceDirect

Journal of Chromatography B

journal homepage: www.elsevier.com/locate/chromb

Comparison of molecular dynamics simulation methods for amyloid β_{1-42} monomers containing D-aspartic acid residues for predicting retention times in chromatography☆

Akifumi Oda[a,b,*], Kana Kobayashi[a], Ohgi Takahashi[a]

[a] Faculty of Pharmaceutical Sciences, Tohoku Pharmaceutical University, 4-4-1 Komatsushima, Aoba-ku, Sendai, Miyagi 981-8558, Japan
[b] Institute for Protein Research, Osaka University, 3-2 Yamadaoka, Suita, Osaka 565-0871, Japan

ARTICLE INFO

Article history:
Received 29 November 2010
Accepted 9 August 2011
Available online 17 August 2011

Keywords:
Molecular dynamics
Implicit solvent
Secondary structure
Amyloid β
Aspartic acid

ABSTRACT

Molecular dynamics simulations of amyloid β_{1-42} containing D-aspartic acid residues were performed using several continuous solvent models to investigate the usefulness of simulation methods for D-amino acid-containing proteins and peptides. Normal molecular dynamics simulations and replica exchange molecular dynamics simulations, which are one of the generalized-ensemble algorithms, were performed. Because the β-structure contents of amyloid β_{1-42} peptides obtained by replica exchange molecular dynamics simulations with Onufriev–Bashford–Case generalized Born implicit solvent were qualitatively consistent with experimental data, replica exchange molecular dynamics rather than other methods appeared to be more reasonable for calculations of amyloid β_{1-42} containing D-aspartic acid residues. Computational results revealed that peptides with stereoinversion of Asp23 tend to form β-sheet structures by themselves, in contrast to the wild-type peptides that form β-sheet structures only after aggregation. These results are expected to be useful for computational investigations of proteins and peptides such as prediction of retention time of peptides and proteins containing D-aspartic acid residues.

1. Introduction

Previously, all amino acids existing in living bodies were believed to have the L-form. However, D-amino acids have recently been found in mammals [1]. In mammals, not only free D-amino acids but also D-amino acid residues that are components of proteins and peptides have been reported. D-Amino acid residues are present in many proteins and peptides, such as amyloid β (Aβ) peptides [2–4], α-crystallin [5], and skin proteins [6]. Among the 20 amino acid residues, nonenzymatic stereoinversions of aspartic acid (Asp) and serine residues are frequently reported. In addition to stereoinversion, isomerization of Asp residues is also frequently observed, and L- and D-β-Asp residues are found in living bodies. It is considered that these stereoinversion and/or isomerization events play important roles in age-related diseases, such as senile cataract, Alzheimer's dementia (AD), and skin aging.

Although the importance of stereoinversion of amino acid residues have been reported, atomic/molecular level investigations have not been sufficiently performed. D-Amino acid residues in proteins and peptides are considered to have effects on the three-dimensional (3D) structures of proteins and peptides. Because denatured proteins and peptides sometimes aggregate, D-amino acid residues are speculated to play important roles in conformational diseases. However, in comparison to native proteins, the solubility of denatured proteins frequently decreases and structural biological experiments, especially atomic-level studies, become difficult. Although the secondary structure contents have been evaluated by circular dichroic (CD) spectroscopy [3,4], atomic-level 3D structures that can be used for structure-based drug design have not been obtained experimentally. Experimental data for 3D structures of Aβ peptides have been reported [7,8]; however, these data include only L-amino acid residues. The experimental 3D structures of Aβ peptides containing D-amino acid residues were not obtained. For structurally unknown proteins and peptides, structural bioinformatics studies, such as molecular simulations

Abbreviations: Aβ, amyloid β; Asp, aspartic acid; AD, Alzheimer's dementia; 3D, three-dimensional; MD, molecular dynamics; GB^{HCT}, generalized Born method developed by Hawkins, Cramer, and Truhlar; REMD, replica exchange molecular dynamics; GB^{OBC}, generalized Born method developed by Onufriev, Bashford, and Case; ALPB, analytical linearized Poisson–Boltzmann method; PSA, polar surface area.

☆ This paper is part of the special issue "Analysis and Biological Relevance of D-Amino Acids and Related Compounds", Kenji Hamase (Guest Editor).

* Corresponding author at: Faculty of Pharmaceutical Sciences, Tohoku Pharmaceutical University, 4-4-1 Komatsushima, Aoba-ku, Sendai, Miyagi 981-8558, Japan, Tel.: +81 22 727 0207; fax: +81 22 275 2013.
E-mail address: oda@tohoku-pharm.ac.jp (A. Oda).

1570-0232/$ – see front matter © 2011 Elsevier B.V. All rights reserved.
doi:10.1016/j.jchromb.2011.08.011

and structural predictions, are frequently useful. Although some molecular dynamics (MD) simulations for wild-type Aβ peptides containing L-amino acid residues were performed [7,9–11], no structural bioinformatics studies for the effect of stereoinversion of amino acid residues have been performed.

Recently, we performed MD simulations of Aβ peptides containing D-Asp residues [12]. In that study, the generalized Born method developed by Hawkins, Cramer, and Truhlar (GB^{HCT}) [13] was used for implicit treatment of water solvent. The results of that study reproduced experimental data in which the tendency of D-Asp-containing Aβ peptides to form β-sheet structures was higher than that of the wild-type peptides. On the other hand, because GB^{HCT} tends to underestimate the effective radii for buried atoms, it may be unsuitable for MD simulations of large proteins containing many buried atoms [14]. Improved versions of GB methods have been developed [15,16], and using these methods more accurate simulations are expected to be performed for large molecules. In this study, MD simulations using several implicit solvent models and two types of initial structures were performed for Aβ peptides containing D-Asp residues and the effects of the solvent models and initial structures were compared. In addition to normal MD simulations, we performed replica exchange MD (REMD) simulations.

Aβ peptides contain 39–43 amino acid residues. Furthermore, these peptides are generated from amyloid precursor proteins [17]. Aβ peptide aggregation is observed in the brains of AD patients, and a relationship between aggregation and AD is speculated. When aggregation occurs, Aβ peptides form β-sheet structures, and interpeptidic interactions are observed between these structures. Presence of apolipoprotein E4 [18], mutations of amino acid residues [19], and cyclization of the side chains of the residues [20] have been proposed as causes of aggregation. Furthermore, a relationship between Aβ aggregation and amino acid residue racemization was considered [2–4]. Because racemization of Asp residues was observed in Aβ peptides extracted from the brains of AD patients, there is a possibility that this racemization is related to AD. Sakai-Kato et al. reported the properties of artificially synthesized $Aβ_{1–42}$ peptides by solid-phase syntheses in which Asp residues were exhaustively substituted with the D-form [4]. Furthermore, they investigated secondary structures and aggregates of peptides and found that β-structure formation and aggregation are triggered by stereoinversion of Asp23 in the $Aβ_{1–42}$ peptide. Because a relationship between $Aβ_{1–42}$ peptide and AD is speculated, structural bioinformatics investigations of the effects of Asp residue stereoinversion on conformations of $Aβ_{1–42}$ peptides are expected to play important roles in AD research.

MD simulations are molecular simulations in which Newton's equation of motion is numerically solved. Using MD simulations, the molecular behavior and optimal structure of molecules under given conditions can be computationally predicted. These methods are used for several types of molecular systems, especially biomolecules. For example, protein–ligand complex structure predictions and protein folding studies have been performed using MD [21]. In addition, retention time predictions of reversed-phase high-performance liquid chromatography (RP-HPLC) for several peptides were carried out by using MD [22]. In MD simulations, solvent water molecules are sometimes not treated explicitly, but implicit solvent models are used. In this study, the usefulness of normal MD and REMD methods using several implicit solvent models and initial structures was investigated.

2. Experimental

2.1. Peptides

In this study, computationally constructed $Aβ_{1–42}$ peptide structures containing 42 residues were used. The two types of initial structures were prepared for the wild-type peptide: one was the experimentally obtained α-helical structure from the Protein Data Bank (PDB ID: 1Z0Q) and the other was the linear structure generated by the tleap module of bug-fixed AmberTools [23]. These initial structures are shown in Fig. 1. Based on the 3D structure of the wild-type peptide (named peptide **1**), the mutant $Aβ_{1–42}$ peptide containing D-Asp23 (peptide **2**), the mutant peptide containing D-Asp1 and D-Asp23 (peptide **3**), and the mutant peptide containing D-Asp7 and D-Asp23 (peptide **4**) were generated. The four peptides used in this study are shown in Table 1. To generate mutants, the side chain atoms except for Cβ in Asp residues were deleted and Cβ was interchanged with Hα. After the interchange, complements of the side chains were generated using tleap. In addition, hydrogen atoms not observed by experiments were added. In our computations, the monomer for each generated peptide was used.

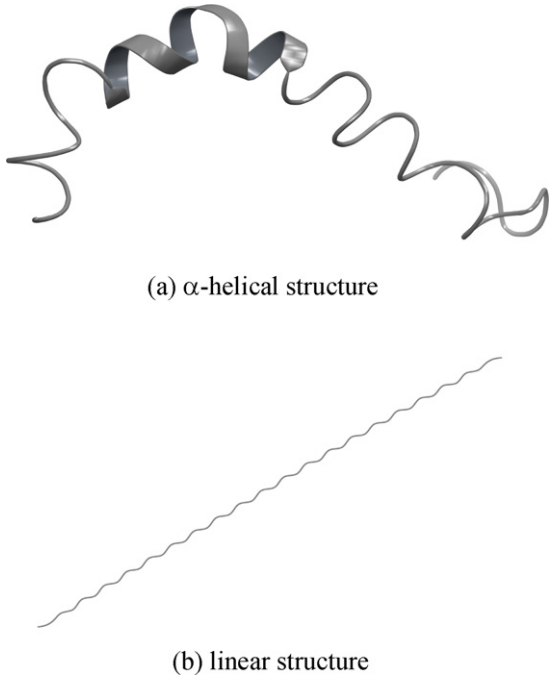

Fig. 1. Initial structures: (a) α-helical structure and (b) linear structure. MD simulations were carried out using these initial structures as starting coordinates. The α-helical initial structure was constructed from the PDB entry 1Z0Q, and the linear initial was constructed by tleap module of AmberTools program. The helix is illustrated by ribbon.

2.2. Computational methods

The structural features of the four types of $Aβ_{1–42}$ peptides were evaluated by MD simulations. For MD calculations, the sander module of bug-fixed AMBER10 [23] was used. The procedures used in this study are summarized in Table 2. As shown in Table 2, MD results calculated using seven types of procedures, which included four types of implicit solvent models, two types of initial structures,

Table 1
Aβ peptides used in this study.

Peptides	D-Amino acid residues	Secondary structure[a]
1	None (wild type)	Random
2	D-Asp23	β sheet
3	D-Asp1, D-Asp23	Random
4	D-Asp7, D-Asp23	β sheet

[a] The secondary structure content was approximately 60% or more in each peptide immediately after dissolution [4].

Table 2
Molecular dynamics (MD) methods used in the test calculations.

Method	Implicit solvent[a]	Initial structure	MD type
I	GB^{OBC} (igb = 2)	α helix	Normal MD
II	GB^{OBC} (igb = 5)	α helix	Normal MD
III	GBn (igb = 7)	α helix	Normal MD
IV	ALPB (alpb = 1, igb = 7)	α helix	Normal MD
V	GB^{OBC} (igb = 5)	Linear	Normal MD
VI	GB^{OBC} (igb = 5)	Linear	REMD
VII	GBn (igb = 7)	Linear	REMD

[a] The values of flags for AMBER input files are given in parentheses.

and a normal MD or REMD, were compared. For MD preparations, first structural minimizations of the added hydrogen atoms were performed and then minimizations of side chains. Next, whole structures were optimized, and the obtained optimized structures were used for MD simulations.

2.2.1. Implicit solvent

For implicit solvent models, the GB model proposed by Onufriev, Bashford, and Case (GB^{OBC}) [15], the GBn model [16], and the analytical linearized Poisson–Boltzmann method (ALPB) [24] were used. In GB models, each atom in a molecule is represented as a sphere of radius R_i with a charge q_i at its center; the interior of the atom is assumed to be filled uniformly with a material of dielectric constant 1. R_i are the so-called effective Born radii. ΔG_{el} is calculated by GB methods as follows:

$$\Delta G_{el} = -\frac{1}{2}\sum_{ij}\frac{q_i q_j}{f_{GB}(r_{ij}, R_i, R_j)}\left(1 - \frac{\exp(-\kappa f_{GB})}{\varepsilon}\right) \quad (1)$$

where r_{ij} is the distance between atoms i and j, and f_{GB} is a certain smooth function of its arguments. κ is the Debye–Hückel screening parameter, and ε is the dielectric constant of solvent. Although the effective Born radius R_i is equal to the van der Waals radius ρ_i for a monoatomic ion, the effective Born radii of buried atoms in intricately shaped molecules should be calculated using some approximation functions. There are some methods for calculations of effective Born radii, and one of the representative methods is Coulomb field approximation (CFA). In CFA, effective Born radii are calculated as follows:

$$R_i^{-1} = \rho_i^{-1} - \frac{1}{4\pi}\int \theta(|\mathbf{r}| - \rho_i) r^{-4} \mathrm{d}\mathbf{r} \quad (2)$$

where the integral is over the solute volume surrounding atom i. For a realistic molecule, the solute boundary (molecular surface) is anything but trivial, and so further approximations are made to obtain a closed-form analytical expression for the above equation, e.g. the so-called pairwise de-screening approach of Hawkins, Cramer and Truhlar [13]. Onufriev, Bashford, and Case improved the method and the modified function to calculate R_i was proposed:

$$R_i^{-1} = \tilde{\rho}_i^{-1} - \rho_i^{-1} \tanh(\alpha\Psi - \beta\Psi^2 + \gamma\Psi^3) \quad (3)$$

where, $\tilde{\rho} = \rho -$ offset and offset is equal to 0.09 Å in Ref. [15]. In the equation, $\Psi = I\tilde{\rho}_i$ and

$$I = \frac{1}{4\pi}\int \theta(|\mathbf{r}| - \tilde{\rho}_i) r^{-4} \mathrm{d}\mathbf{r} \quad (4)$$

In this equation, α, β, and γ are treated as adjustable dimensionless parameters to be optimized. Onufriev, Bashford, and Case proposed two types of parameter settings, $\alpha = 0.8$, $\beta = 0.0$, and $\gamma = 2.909125$ ("igb = 2″ setting), and $\alpha = 1.0$, $\beta = 0.8$, and $\gamma = 4.85$ ("igb = 5″ setting). Another improved version of GB, GBn, in which a simple analytic correction term is introduced for solvent-excluded volume of each pair of atoms, has been proposed. In addition to GB, ALPB method is one of the promising approaches of continuous solvent. ALPB equation approximates ΔG_{el} as

$$\Delta G_{el} = -\frac{1}{2}\left(\frac{1}{\varepsilon_{in}} - \frac{1}{\varepsilon_{ex}}\right)\frac{1}{1+\alpha\beta}\sum_{ij} q_i q_j \left(\frac{1}{f_{GB}} + \frac{\alpha\beta}{A}\right) \quad (5)$$

where $\beta = \varepsilon_{in}/\varepsilon_{ex}$ is the ratio of the internal and external dielectrics, $\alpha = 0.571412$, and A characterizes the over-all dimensions and global shape, so-called effective electrostatic size of the molecule. In this study, two types of settings, i.e., $\alpha = 0.8$, $\beta = 0.0$, and $\gamma = 2.909125$ ("igb = 2″ setting) as well as $\alpha = 1.0$, $\beta = 0.8$, and $\gamma = 4.85$ ("igb = 5″ setting), were examined for GB^{OBC}. These parameters have been tested by Onufriev, Bashford, and Case, and they are widely used for MD simulations. These settings are only two allowed settings of GB^{OBC}. The effective electrostatic size for ALPB was determined to be 20 Å from the result of utility *elsize* calculation. The effective Born radii for ALPB were obtained from GBn. For the implicit solvent models, salt concentrations for ion screening of interactions by the Debye–Hückel limiting law were set to 0.1 M. The atomic radii of mbondi2, which is prepared from the Bondi set [25] by increasing the radius of every hydrogen atom bound to a nitrogen from 1.2 to 1.3 Å [15], were used for GB^{OBC} and Bondi radii [25] were used for GBn and ALPB.

2.2.2. General MD parameters

The maximum number of cycles were set at 500, 10,000, and 30,000 for minimization of hydrogen atoms, side chains, and whole molecules, respectively. Minimizations were terminated when the energy gradient was less than 0.1 kcal/mol Å. Minimizations for hydrogen atoms and side chains were performed in vacuo because of the limitation of AMBER10, and whole molecule minimizations were performed in implicit solvents. For normal MD, total 100-ns simulations were performed using a 1-fs time step at 300 K. In addition to normal MD, REMD calculations were performed. In REMD, structure sampling can be more widely performed than that in normal MD because high-temperature simulations are performed together with low-temperature simulations. In this study, REMD was used for simulations with a linear initial structure. Because the linear peptide structure appears to be different from the native structure, expanded ensemble methods such as REMD that can powerfully sample the structures should be examined. For linear initial structures, 2000-cycle minimizations were performed before REMD calculations. The multiple MD simulations at different temperatures were performed in parallel for REMD. In this study, 16 temperatures were used: 269.7 K, 284.4 K, 300.0 K, 316.4 K, 333.8 K, 352.0 K, 371.3 K, 391.7 K, 413.1 K, 435.7 K, 459.6 K, 484.8 K, 511.3 K, 539.3 K, 568.8 K, and 600.0 K. These temperatures were exponentially distributed, and the exponential distribution of temperatures is generally used setting for REMD [26]. In preparation for REMD, 200-ps normal MD simulations with a 2-fs time step were performed to achieve equilibria at given temperatures. Then, 50-ns REMD calculations with a 2-fs time step were performed. The number of MD steps between each exchange attempt was set to 500. Because high-temperature MD calculations were included in REMD, artificial (undesirable) chiral inversions frequently occurred. Thus, structural restrictions using initial structures were adopted to avoid chiral inversions.

The covalent bonds containing hydrogen atoms were restricted by SHAKE [27]. AMBER ff99SB force field [28,29] was used for all calculations. For the force field parameters of D-Asp residues, values same as those used for L-Asp residues were adopted. The cutoff length of nonbonding interactions was set to 999 Å, and the maximum distance between atom pairs that will be considered in pairwise summation involved in calculating the effective Born radii was also equal to 999 Å. Because the interatomic distances

in $A\beta_{1-42}$ never exceeded 999 Å throughout the calculations, these cutoff values were equivalent to no cutoff.

2.2.3. Analyses

MD results were analyzed using the ptraj module of AmberTools. The structures of $A\beta_{1-42}$ peptides were extracted every 0.5 ps (for normal MD) or 1.0 ps (for REMD), and secondary structures for all residues of the extracted peptide structures were assigned by the DSSP method [30]. For structural analyses, MD trajectories after 50 ns (for normal MD) or after 20 ns (for REMD) were used. The secondary structure contents of peptides were calculated using the DSSP results, and the tendencies of residues to form some particular secondary structures were also investigated.

2.2.4. Comparison between MD results and retention time in RP-HPLC

In addition to benchmark tests of MD simulations, the comparisons between MD results and experimental retention time in RP-HPLC were carried out as practical examples. For the comparisons, the peptide corresponding to amino acids 70–88 (KFVIFLDVKHFSPEDLTVK) of human αA-crystallin [31] was used. Two types of the peptides were computationally constructed for our tests; one includes L-Asp as Asp76, and the other includes D-Asp as Asp76. MD simulations for both of the constructed peptides were performed, and the structural properties obtained by the simulations were compared with experimental retention times. The retention times obtained by RP-HPLC experiments were 95.2 min for L-Asp76 containing peptide and 93.2 min for D-Asp76 containing peptide [31]. For the MD simulations, the method **IV** was used and the parameter settings were same as the MD for $A\beta_{1-42}$ peptide mentioned in Sections 2.2.1 and 2.2.2. After MD simulations, structural properties of the two peptides were analyzed. The amino acid sequence, hydrophobicity, and molecular size of peptides were already known to influence the retention time [32]. Although the values of regression coefficients were different for different HPLC conditions, qualitative tendencies are known; larger size and less hydrophobicity of peptides decrease the retention time [33]. Thus, in this study, polar surface area (PSA) percentage and molecular volume were calculated, and these values were qualitatively compared with experimental retention time. Because high correlation between PSA percentage and log *P* was reported [34], PSA percentage was used as the indicator value for hydrophobicity. PSA was calculated using DMS program [35,36], and the percentage of PSA in whole surface was defined as PSA percentage. The log *P* values were obtained by PSA percentages, using the regression expression derived from the data in Ref. [34]. The molecular volume was calculated by Mol_Volume program [37]. For these calculations, probe radius was set to 1.4 Å. 3D structures of peptides were extracted from MD trajectories after 50 ns, and the average values were obtained both for PSA percentage and for molecular volume.

3. Results and discussion

3.1. Secondary structure contents

At first, the β-structure and random coil contents were calculated for comparison between results of MD simulations and experimental data. The secondary structure contents were computed from the number of residues with certain secondary structures and the number of all residues as follows:

$$P_{\text{beta}} = \frac{N_{\text{beta}}}{N_{\text{all}}} \quad (6)$$

$$P_{\text{random}} = \frac{N_{\text{random}}}{N_{\text{all}}} \quad (7)$$

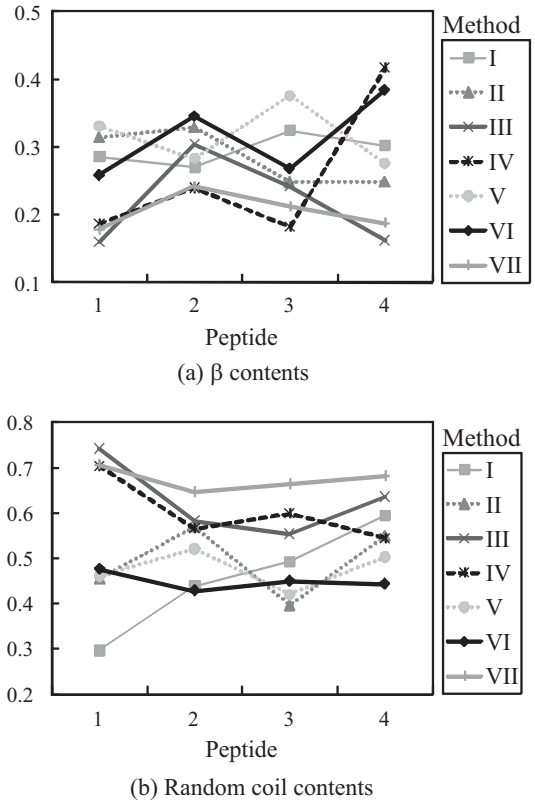

Fig. 2. Comparisons of the secondary structure contents. Secondary structures were defined by DSSP program included in ptraj module of AmberTools. The vertical axes of the figure are the secondary structure contents. (a) β contents and (b) random coil contents.

where P_{beta} and P_{random} were the β-structure contents and random coil contents, respectively. N_{beta}, N_{random}, and N_{all} were the number of β-structure residues, random coil residues, and all residues, respectively. For calculations of the secondary structure contents, the residues classified as "b" (parallel β sheet), "B" (antiparallel β sheet), and "T" (hydrogen bonded turn) were defined as β-structure residues. The residues classified as "0" (random coil) were defined as random coil residues. The definitions of secondary structures are same as those used in Ref. [11] and reflect the fact that the experimental β-structure contents include β-turn contents [38]. In Fig. 2, the secondary structure contents obtained by seven MD simulations are shown. In addition, the values of secondary structure contents are described in Table S1 of Supplementary data. The values illustrated in the figure are the averages throughout MD trajectories. Experimentally observed helix, β, and random coil contents for wild-type peptide **1** were approximately 5%, 25%, and 70%, respectively [4,38]. Furthermore, experimentally observed β content for peptide **2**, in which Asp23 was sterically inverted, was approximately 60% [4]. In the comparison between the calculated results of peptides **1** and **2**, β contents obtained by methods **II**, **III**, **IV**, **VI**, and **VII** for peptide **2** were larger than those for peptide **1** (Fig. 2). On the other hand, for random coil contents, methods **III**, **IV**, **VI**, and **VII** provided qualitatively reasonable results in which the contents for peptide **1** were larger than those for peptide **2**. Because methods **III**, **IV**, **VI**, and **VII** can qualitatively reproduce both β and random coil contents, these methods appear capable of reasonably calculating the effect of stereoinversion of Asp residues on 3D structures. Considering not only peptides **1** and **2** but also **3** and **4**, only two methods, **IV** and **VI**, can qualitatively reproduce the experimental results in which β contents of peptides **2** and **4** were larger than those of peptides **1** and **3** and random coil contents of peptides **1** and **3** were larger than those of **2** and **4**. Although the

computational results of method **VII** were consistent with experiments for peptides **1**, **2**, and **3**, the results for the β contents of peptide **4** were inconsistent.

Method **IV** could reproduce the experimental results; however, random coil contents were overestimated by this method. For example, the calculated random coil content of peptide **2** by this method was 56.5%, although the experimental random coil content was smaller than approximately 40%. In this study, the setting "igb = 7″ was used for method **IV**. The random coil contents obtained by other methods using the "igb = 7″ setting, i.e., methods **III** and **VII**, were also larger than those of method **VI**; the random coil content of peptide **2** by method **III** was 58.2% and by method **VII** was 64.6%, although that by method **VI** was 42.8%. In addition to random coil contents, β contents calculated by method **IV** were much smaller than those calculated by method **VI** except for peptide **4**, although method **IV** could reproduce β contents qualitatively. In particular, for peptide **2**, the β content obtained by method **IV** was 23.9%, and it was the smallest value obtained among the methods. These results suggest that secondary structure formation was restrained and random coil structure was overestimated in the "igb = 7″ setting. On the other hand, random coil contents calculated by method **VI** were not unacceptably high for peptides **2** and **4**, for which the experimental contents were smaller than approximately 40%. The calculated random coil contents obtained by method **VI** for these two peptides were the smallest among the methods used in this study. In addition to the random coil contents, although the β content of peptide **2** calculated by method **VI** was smaller than the experimental value, it was closest to the experimental value as shown in Fig. 2. These results indicate that method **VI** is the most appropriate method to calculate the structural features of $A\beta_{1-42}$ peptides.

For the β and random coil contents, the results obtained by method **I**, in which more β structures were observed in peptides **1** and **3** and more random coils were present in peptides **2** and **4**, were inconsistent with the experimental results, suggesting that method **I** is inappropriate for evaluating the secondary structures of $A\beta_{1-42}$ peptides. On the other hand, the β contents obtained by method **II** were comparatively reasonable for peptides **1**, **2**, and **3**. Although the GB^{OBC} implicit solvent was used in methods **I** and **II**, the secondary structure contents obtained by method **II** were closer to the experimental results. Thus, the "igb = 5″ setting appeared to be reasonable for GB^{OBC}.

The secondary structure contents calculated by method **V** in which the linear initial structure was used were unreasonable because they did not reproduce the experimental data. As discussed previously, method **II**, which used the same settings as method **V** except for the initial structure, gave partially reasonable results. These results indicate that the effect of the initial structures cannot be eliminated by 100-ns normal MD. In particular, because the β contents calculated by method **V** were different from those calculated by method **II**, hydrogen-bonding networks appeared to be affected by the initial structures. In contrast to normal MD, REMD with linear initial structures (method **VI**) can reproduce the experimental results qualitatively, although the settings were the same as those for method **V**. The results suggest that REMD is useful even if highly artificial initial structures were used, and powerful sampling methods such as REMD should be applied for artificially generated initial structures. In addition, the results also indicate that 50-ns REMD simulations can provide reasonable results, although 100-ns normal MD is insufficient.

The results illustrated in Fig. 2 were calculated for monomer $A\beta_{1-42}$ peptides, and the REMD-calculated β content for peptide **2** was higher than that for peptide **1** in the monomer state. These are similar to the results obtained in Ref. [12], and indicate that peptide **2** forms a β structure without aggregation. This finding is consistent with the experimental observations in which the β content of peptide **2** was higher than that of peptide **1** immediately after dissolution. On the other hand, the absolute value of the β content for peptide **2** was smaller than the experimental value (approximately 60%), even when method **VI**, which can reproduce the experimental results qualitatively, was used. This result may be because of the limitations of the implicit solvent and/or the ff99SB force field. Because the hydrogen-bonding pattern including water molecules plays important roles in secondary structure formation, the explicit water molecules may be more suitable for quantitatively accurate simulations, although implicit water models can reproduce experiments qualitatively. In addition, the ff99 force field is known to overestimate helical structures. Although ff99SB is the modified version of ff99, the tendency to form a helix may influence the results. We intend to investigate these aspects further in a future study via simulations using the explicit solvent and/or other force fields.

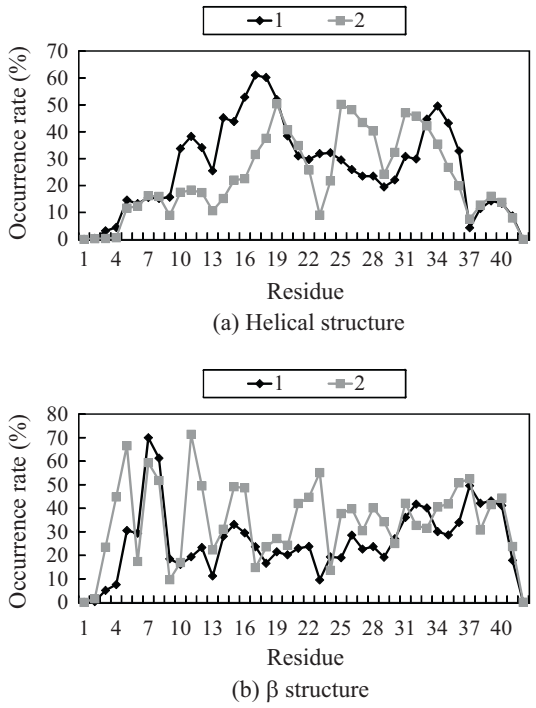

Fig. 3. Occurrence ratios of secondary structures for residues obtained by REMD. The ratios were calculated by N_{sec}/N_{all}, where N_{sec} is the number of snapshots in which the secondary structure appeared in the residue, and N_{all} is the number of all snapshots used for analyses (in case of REMD, N_{all} = 30,000). (a) Helical structure and (b) β structure. In these figures, "**1**" and "**2**" indicate the occurrence ratios for each residue of peptides **1** and **2**, respectively.

3.2. Occurrence ratios of secondary structures for each residue

The occurrence ratios of helical and β structures for each residue of peptides **1** and **2** calculated from MD trajectories by method **VI**, which can qualitatively reproduce experimental results, are shown in Fig. 3. The helical structures include α, 3_{10}, and π helices and β structures include parallel and antiparallel sheets as well as hydrogen-bonded turns. As shown in the figure, not only the occurrence ratio of β structures in the C-terminal region but also in the N-terminal region for peptide **2** was larger than that for peptide **1**. Thus, large parts of the $A\beta_{1-42}$ monomer appeared to form β structures by stereoinversion of Asp23. The peak of the helical structures located in the C terminus of peptide **1** shifted from residue 34 to 31, and the result indicates that the tendency of the C-terminal region of $A\beta_{1-42}$ to form helical structures is decreased because of the presence of D-Asp23. Because the C-terminal helix is known to play important roles in the aggregation of wild-type Aβ [7,39],

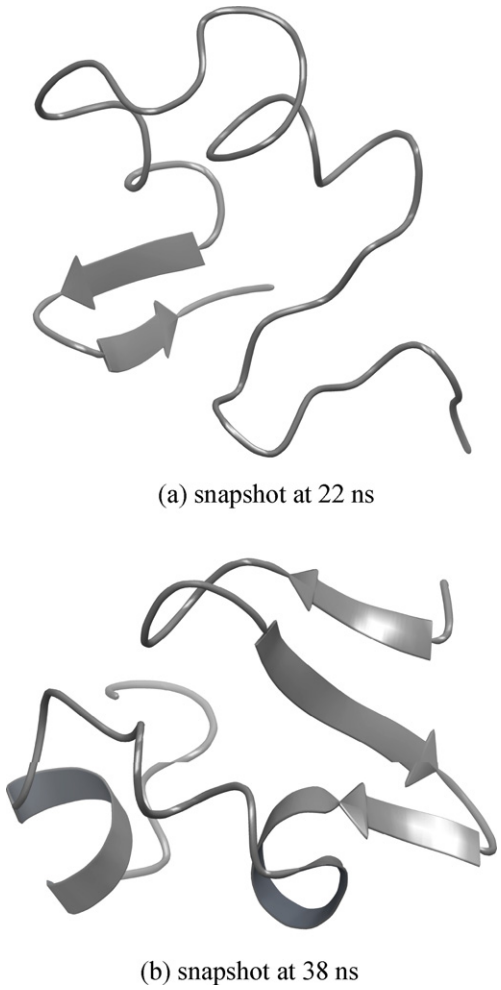

Fig. 4. Two snapshots in trajectory for peptide **2** obtained by method **i**. The β structures were observed in C-terminal region for the snapshot at 22 ns, and in N-terminal region for the snapshot at 38 ns.

the difference in C-terminal secondary structures between peptides **1** and **2** may suggest that the mechanism of aggregation for Aβ containing D-Asp residues is different from that of wild-type.

In Fig. 4, the representative 3D structures of $A\beta_{1-42}$ containing D-Asp23 (peptide **2**) obtained by the MD simulation using method **VI** are shown. In the figure, snapshot structures at 22 and 38 ns, in which β structures were observed, are illustrated. The helical and arrowed ribbons represent the α helix and β sheet, respectively. As shown in the figure, β structures were clearly observed in the C-terminal region for snapshot (a) and in the N-terminal region for snapshot (b).

3.3. Relationship between MD results and retention time for αA-crystallin 70–88 peptides

In order to investigate usefulness of MD simulation for peptides including D-Asp residues, the comparison between the results of MD simulations and experimental retention time by RP-HPLC [31] was carried out for αA-crystallin 70–88 peptides. In Table 3, molecular volumes and PSA percentages of calculated peptide structures obtained by MD simulations are shown. The values were the ensemble average of MD trajectories after 50 ns. The predicted log *P* values by the regression expression derived from data in Ref. [34] were also described. In addition, the experimental values of retention times observed by Fujii et al. [31] are also shown in Table 3. Experimental conditions of RP-HPLC adopted in Ref. [31] were as follows: Column; C18 column (Shiseido CAPCELL PAK UG80 3.0 mm × 250 mm), eluent; 0.1% trifluoroacetic acid in water (A) and 0.1% trifluoroacetic acid in acetonitrile (B), gradient; 0-60% B in 170 min, flow rate 0.5 ml/min. As shown in the table, the molecular volume of the peptide including D-Asp76 was larger than that of the peptide including L-Asp76, and the hydrophobicity of D-Asp76 peptide was lower than that of L-Asp76 peptide. These changes of molecular properties were caused by the changes of molecular structures induced by stereoinversion of Asp76 residue. Since the larger molecular volume and less hydrophobicity tend to decrease the retention time by RP-HPLC [32], the molecular properties shown in Table 3 are qualitatively consistent with the experimental results shown in Ref. [31]. There were no studies for the calculations of molecular volumes and PSA for D-Asp including peptides using MD simulations until now. The results shown in Table 3 indicate that MD simulations are useful for the calculations of these physicochemical properties of D-Asp including peptides. As mentioned above, because these properties are known to be related to retention time by RP-HPLC, MD simulations have possibility for retention time prediction of peptides including D-amino acid residues.

For the quantitative prediction of the retention time, because the regression expressions have to be derived from experimental data observed under certain HPLC condition, a large number of experimental data obtained under certain condition have to be gathered. As shown in Ref. [33], very different regression coefficients are derived from different HPLC conditions. In addition, in the amino-acid-sequence-dependent term included in the regression expression (Sum_{AA} term of Ref. [32]), there is no parameter for the D-Asp residue. Therefore, a large number of experimental data for D-Asp including peptides obtained under certain HPLC condition are indispensable for quantitative predictions of retention time, although only a few number of data have been obtained for D-Asp including peptides at present. On the other hand, the results of our study may provide some validations for usefulness of MD simulations for retention time predictions of D-Asp including peptides. As shown in Table 3, the descriptors for retention time predictions, such as molecular volume and hydrophobicity, may be prepared by MD simulations. As shown in Ref. [33], the coefficients of log Sum_{AA}, molecular volume, and log *P* were from 9.3821 to 50.3284, from −18.3694 to −5.0671, and from 0.2684 to 2.6027, respectively. When the larger values of the coefficients are used, the contribution of molecular volume and log *P* to the difference of retention times between the L-Asp76 and the D-Asp76 including peptides (Δt_R) can be predicted to be around 0.4 min. As mentioned above, the contribution of Sum_{AA} cannot be estimated because there is no parameter for the D-Asp residue. However, if the difference in the log Sum_{AA} term between the L-Asp76 and the D-Asp76 including peptides is

Table 3
Molecular volume, polar surface area (PSA) percentage, and predicted log *P* of αA-crystallin 70–88 peptides.

	Molecular volume (Å^3)	PSA percentage	log *P*[a]	Retention time (min)[b]
L-Asp76 including peptide	5037	26.5%	−0.671	95.2
D-Asp76 including peptide	5165	27.0%	−0.743	93.2

[a] Calculated by the regression analysis of the data in Ref. [34].
[b] Experimentally observed retention time reported in Ref. [31].

around 0.05, the contribution of $\log \mathrm{Sum}_{AA}$ to Δt_R may be 1 min or more. Because the experimental Δt_R was equal to 2.0 min, the summation of the contributions of $\log \mathrm{Sum}_{AA}$, molecular volume, and $\log P$ might explain the Δt_R quantitatively. In the future, quantitative regression expressions are expected to be derived from experimental HPLC data and MD results, when many HPLC experiments are carried out for D-Asp including peptides. The retention time predictions for D-Asp including peptides cannot be performed by the method using only amino acid sequence [40], because the peptide conformations play important roles in retention time. In addition, retention time prediction using Gibbs energy calculations [22] spend huge computational costs. Thus, the regression expression derived from normal MD simulations and experimental data are expected to be useful for retention time predictions of D-Asp including peptides.

4. Conclusions

In this study, MD simulations for $A\beta_{1-42}$ peptides containing D-Asp residues were performed using several implicit solvent models. In addition to normal MD, REMD was performed. The computational results were compared with experimental data obtained by CD spectra, and the usefulness of MD procedures was evaluated. The results indicate that REMD with GB^{OBC} is useful for simulations of D-Asp-containing peptides. In addition, because force field parameters for L-Asp residues were used for D-Asp residues without modification in this study, the qualitatively reasonable results obtained by REMD suggest that the existing force fields can also be applied for calculations of D-amino acid-containing peptides. For normal MD calculations, ALPB using GBn radii appears to be appropriate. On the other hand, results of the "igb = 2" setting of GB^{OBC} were inconsistent with experimental data, and the "igb = 5" setting was more suitable for GB^{OBC}. As shown in the results of the simulations using linear initials, because the effect of initial structures was larger for normal MD than for REMD, REMD appears to be appropriate if reasonable initial structures cannot be prepared. The results of this study are considered guidelines for the simulations of proteins and peptides containing D-amino acid residues, and structural bioinformatics investigations of these peptides are expected to be performed by reference to the results of this study. MD simulations are useful not only for secondary structure predictions mentioned in this study, but also for the investigations of other structural features, such as the evaluations of hydrophobicities which are influenced by 3D structures.

The results of this study suggest that the monomer peptide **2** forms β-sheet structures by itself, and the results were consistent with the experimental data in which β structures were observed immediately after dissolution. Because peptide **1** is known to form β-sheet structures after aggregation [41], the computational results in which peptide **2** forms β-sheet structures without aggregation indicate that the mechanisms of β-sheet formation were different between peptides **1** and **2**.

Acknowledgment

Parts of the computations were performed by the Research Center for Computational Science, Okazaki and the Research Institute for Information Technology, Kyushu University.

Appendix A. Supplementary data

Supplementary data associated with this article can be found, in the online version, at doi:10.1016/j.jchromb.2011.08.011.

References

[1] N. Fujii, T. Saito, Chem. Rec. 4 (2004) 267.
[2] A.E. Roher, J.D. Lowenson, S. Clarke, C. Wolkow, R. Wang, R.J. Cotter, I.M. Reardon, H.A. Zürcher-Neely, R.L. Heinrikson, M.J. Ball, B.D. Greenberg, J. Biol. Chem. 268 (1993) 3072.
[3] T. Tomiyama, S. Asano, Y. Furiya, T. Shirasawa, N. Endo, H. Mori, J. Biol. Chem. 269 (1994) 10205.
[4] K. Sakai-Kato, M. Naito, N. Utsunomiya-Tate, Biochem. Biophys. Res. Commun. 364 (2007) 464.
[5] N. Fujii, K. Satoh, K. Harada, Y. Ishibashi, J. Biochem. 116 (1994) 663.
[6] N. Fujii, S. Tajima, N. Tanaka, N. Fujimoto, T. Takata, T. Shimo-Oka, Biochem. Biophys. Res. Commun. 294 (2002) 1047.
[7] S. Tomaselli, V. Esposito, P. Vangone, N.A.J. van Nuland, A.M.J.J. Bonvin, R. Guerrini, T. Tancredi, P.A. Temussi, D. Picone, ChemBioChem 7 (2006) 257.
[8] T. Lührs, C. Ritter, M. Adrian, D. Riek-Loher, B. Bohrmann, H. Döbeli, D. Schubert, R. Riek, Proc. Natl. Acad. Sci. U.S.A. 102 (2005) 17342.
[9] A. Baumketner, S.L. Bernstein, T. Wyttenbach, G. Bitan, D.B. Teplow, M.T. Bowers, J.-E. Shea, Protein Sci. 15 (2006) 420.
[10] A. Kent, A.K. Jha, J.E. Fitzgerald, K.F. Freed, J. Phys. Chem. 112 (2008) 6175.
[11] J. Ikebe, N. Kamiya, J. Ito, H. Shindo, J. Higo, Protein Sci. 16 (2007) 1596.
[12] A. Oda, K. Kobayashi, O. Takahashi, Chem. Biodivers. 7 (2010) 1357.
[13] G.D. Hawkins, C.J. Cramer, D.G. Truhlar, J. Phys. Chem. 100 (1996) 19824.
[14] A. Onufriev, D. Bashford, D.A. Case, J. Phys. Chem. B 104 (2000) 3712.
[15] A. Onufriev, D. Bashford, D.A. Case, Proteins: Struct. Funct. Bioinf. 55 (2004) 383.
[16] J. Mongan, C. Simmerling, J.A. McCammon, D.A. Case, A. Onufriev, J. Chem. Theory Comput. 3 (2006) 156.
[17] J. Kang, H.-G. Lemaire, A. Unterbeck, J.M. Salbaum, C.L. Masters, K.-H. Grzeschik, G. Multhaup, K. Beyreuther, B. Mullaer-Hill, Nature 325 (1987) 733.
[18] E.H. Corder, A.M. Saunders, W.J. Strittmatter, D.E. Schmechel, P.C. Gaskell, G.W. Small, A.D. Roses, J.L. Haines, M.A. Pericak-Vance, Science 261 (1993) 921.
[19] T. Wisniewski, J. Ghiso, B. Frangione, Biochem. Biophys. Res. Commun. 179 (1991) 1247.
[20] T.C. Saido, T. Iwatsubo, D.M. Mann, H. Shimada, Y. Ihara, S. Kawashima, Neuron 14 (1995) 457.
[21] D.A. Case, T. Cheatham, T. Darden, H. Gohlke, R. Luo, K.M. Merz Jr., A. Onufriev, C. Simmerling, B. Wang, R. Woods, J. Comput. Chem. 26 (2005) 1668.
[22] C.-W. Tsai, C.-I. Liu, Y.-C. Chan, H.-H.G. Tsai, R.-C. Ruaan, J. Phys. Chem. B 114 (2010) 11620.
[23] D.A. Case, T.A. Darden, T.E. Cheatham III, C.L. Simmerling, J. Wang, R.E. Duke, R. Luo, M. Crowley, R.C. Walker, W. Zhang, K.M. Merz, B. Wang, S. Hayik, A. Roitberg, G. Seabra, I. Kolossváry, K.F. Wong, F. Paesani, J. Vanicek, X. Wu, S.R. Brozell, T. Steinbrecher, H. Gohlke, L. Yang, C. Tan, J. Mongan, V. Hornak, G. Cui, D.H. Mathews, M.G. Seetin, C. Sagui, V. Babin, P.A. Kollman, AMBER 10, University of California, San Francisco, 2008.
[24] G. Sigalov, A. Fenley, A. Onufriev, J. Chem. Phys. 124 (2006) 124902.
[25] A. Bondi, J. Phys. Chem. 68 (1964) 44.
[26] H. Nymeyer, S. Gnanakaran, A.E. García, Methods Enzymol. 383 (2004) 119.
[27] J.-P. Ryckaert, G. Ciccotti, H.J.C. Berendsen, J. Comput. Phys. 23 (1997) 327.
[28] J. Wang, P. Cieplak, P.A. Kollman, J. Comput. Chem. 21 (2000) 1049.
[29] V. Hornak, R. Abel, A. Okur, B. Strockbine, A. Roitberg, C. Simmerling, Proteins: Struct. Funct. Bioinf. 65 (2006) 712.
[30] W. Kabsch, C. Sander, Biopolymers 22 (1983) 2577.
[31] N. Fujii, N. Fujii, M. Kida, T. Kinouchi, Amino Acids 39 (2010) 1393.
[32] R. Kaliszan, T. Bączek, A. Cimochowska, P. Juszczyk, K. Wiśniewska, Z. Grzonka, Proteomics 5 (2005) 409.
[33] T. Bączek, P. Wiczling, M. Marszałł, Y.V. Heyden, R. Kaliszan, J. Proteome Res. 4 (2005) 555.
[34] D. Barlow, T. Satoh, J. Control. Release 29 (1994) 283.
[35] F.M. Richards, Ann. Rev. Biophys. Bioeng. 6 (1977) 151.
[36] C. Huang, DMS, University of California, San Francisco, 2002.
[37] A. Balaeff, Mol.Volume, University of Illinois, Urbana-Champaign, 2001.
[38] Y. Fezoui, D.B. Teplow, J. Biol. Chem. 277 (2002) 36948.
[39] C.J. Pike, D. Burdick, A.J. Walencewicz, C.G. Glabe, C.W. Cotman, J. Neurosci. 13 (1993) 1676.
[40] J.L. Meek, Proc. Natl. Acad. Sci. U.S.A. 77 (1980) 1632.
[41] M. Kirkitadze, M.M. Condron, D.B. Teplow, J. Mol. Biol. 312 (2001) 1103.